J Cancer Res Clin Oncol (2004) 130: 15–24
DOI 10.1007/s00432-003-0491-1

ORIGINAL PAPER

Daniel Tee · Joseph DiStefano III

Simulation of tumor-induced angiogenesis and its response to anti-angiogenic drug treatment: mode of drug delivery and clearance rate dependencies

Received: 10 February 2003 / Accepted: 29 July 2003 / Published online: 28 October 2003

Abstract Tumor cells secrete diffusible substances collectively called tumor angiogenic factors (TAFs), most notably vascular endothelial growth factor (VEGF) and basic fibroblast growth factor (bFGF), which in turn stimulate endothelial cell migration and thus angiogenesis, or new blood vessel formation. Anti-angiogenic drugs for cancer treatment are receiving much attention, with endostatin identified as one of the potent inhibitors. Although the mechanisms of action of endostatin are yet to be fully elucidated, there is evidence that bFGF and endostatin may bind competitively to heparan sulfate proteoglycan receptors on endothelial cells, or endostatin may otherwise downregulate bFGF or VEGF and its receptors, putatively inhibiting cell proliferation. To test these and other hypotheses of inhibitory action that can be similarly formulated, for other TAF inhibitors as well as endostatin, we have developed a mathematical model of extratumoral angiogenesis in cancer in response to specific anti-angiogenic drug treatment. It is built on previous work, a modification and augmentation of published models, and is expressed as four nonlinear partial differential equations, with specific terms for endothelial cell proliferation, degradation, and endostatin-TAF inhibition, and a stochastic, discretized version of this model to represent vessel growth. Our extended model reproduces the simulated kinetics of angiogenesis in a mouse tumor model reported earlier. We assessed the anti-angiogenic kinetic behavior of our extended model by simulating dynamic responses to exogenous endostatin treatment in the same mouse model, using four dosage regimens, two of these reported for in vivo pre-clinical or clinical studies, and two 10 times greater: daily single bolus injections of 20 mg/kg per day and 200 mg/kg per day, and constant infusions of 20 mg/kg per day and 200 mg/kg per day, each for 20 simulated days. We also explored the effects of drug clearance, over an eightfold range of clearance rates that include scaled clearances for endostatin, a sister-drug angiostatin, or similar drugs with clearances in this range. Predictively, our simulation results suggest ineffectiveness of the bolus injection protocols, consistent with in vivo data with angiostatin treatment, whereas simulated constant infusion of endostatin in the mouse model effectively suppresses angiogenesis after only 3 days of treatment, at the lowest dose, over a wide range of drug clearance rates.

Keywords Endostatin · Angiostatin · Dosing · Mathematical model · Endothelial cell · Heparan

D. Tee · J. DiStefano III (✉)
Departments of Computer Science and Medicine, 4711 Boelter Hall, UCLA, Los Angeles, CA 90095–1596, USA
E-mail: joed@cs.ucla.edu
Fax: +1-310-7945057

Introduction

Angiogenesis is the formation of new blood vessels from pre-existing vasculature in response to some extracellular stimuli. Blood vessel growth is initially driven by endothelial cell migration, and then the cells organize themselves into dendritic structures. In tumorigenesis, angiogenesis plays a pivotal role in determining the transformation of tumor cells from a dormant avascular state to a harmful vascular state (Folkman and Klagsburn 1987; Griffioen and Molema 2000).

Much evidence has shown that angiogenesis is a result of the intricate interaction of various physiological subsystems, including those controlling *vascular endothelial growth factors* (VEGF), and coagulation and plasminogen subsystems. Tumor cells secrete *tumor angiogenic factors* (TAFs), most notably VEGF and *basic fibroblast growth factors* (bFGF), which promote neovascularization via penetration of neighboring blood vessels, thereby providing them with an adequate blood supply and the nutrients needed for further carcinogenic progression (Folkman and Klagsburn 1987). An avascular cluster of tumor cells typically consists of a central inactive core of dying cells, surrounded by an outer layer

of proliferating cells, which cannot grow beyond a few millimeters due to limited diffusibility of nutrients. A tumor consumes nutrients at a rate proportional to its volume, whereas the diffusibility of nutrients is only proportional to its surface area. However, with the penetration of new blood vessels, tumor cells can efficiently obtain nutrients needed for their development. And once a cluster of tumor cells progresses to the vascular state, it can grow much larger, thereby gaining the ability to fragment from the cluster, and metastasize in other parts of body (Orme and Chaplain 1996).

Tumor-induced angiogenesis involves three major sub-processes: 1) degradation of the basement membrane by enzymes secreted by endothelial cells; 2) migration of endothelial cells along the gradient of several substances, one of these being *fibronectin* (Fn), a major component of the extracellular matrix; and 3) proliferation of endothelial cells. These are distinct events, each triggered by different stimuli (Orme and Chaplain 1997; Griffioen and Molema 2000).

Degradation of the basement membrane begins when the tumor cells release *tumor angiogenic factors* (TAFs), which then diffuse through the extracellular matrix, resulting in a gradient of TAFs between the tumor cell cluster and existing blood vessels, where they bind to surface receptors. TAFs then induce the endothelial cells of the vessel wall to thicken and reorganize themselves into finger-like protrusions. This also promotes endothelial cell secretion of proteases, which in turn degrade the parent venule basement membrane, loosening endothelial cell connections with their neighbors. The detached cells then migrate toward the tumor cells (Orme and Chaplain 1997).

Migration of endothelial cells is influenced by three factors: random motility, and concentration gradients of TAF and Fn. *Random motility* refers to simple diffusion of endothelial cells in the absence of any attracting or inhibiting substances. When TAFs are present, endothelial cells migrate in the direction of increasing TAF concentrations, a process called *chemotaxis* (Chaplain and Stuart 1993). Similarly, the affinity of endothelial cells to follow Fn gradients is called *haptotaxis*. Fn is not readily diffusible, exerting its haptotactic effect by binding to *integrins* on the cell surface. Then, anchorment of endothelial cells onto the extracellular matrix, with the assistance of Fn, promotes migration of endothelial cells and attachment of branching vessels; and binding of Fn also promotes mitosis (Ingber 1990).

Following their migration, endothelial cells accumulate in the region where the concentration of TAFs reaches a certain threshold level, and the blood vessel wall begins to bulge, initiating a new sprout, which then grows in length, to further recruit endothelial cells. Eventually, the cells immediately behind the sprout tip begin to proliferate. The repeated process of migration, sprout extension and cell proliferation constitutes the growth process for new blood vessels.

Recombinant human rhE-Endostatin (*Pichia pastoris*; Entremed, Rockville, MD), the putative angiogenesis inhibitory drug under primary consideration here, is a manufactured version of naturally occurring, tumor-derived endostatin, a 22-kDalton fragment of collagen XIII (O'Reilly et al. 1997). The mechanism of action of endostatin is not well established, but it is believed to exert its anti-angiogenic effect by inhibiting mitogen-stimulated proliferation of endothelial cells. Among other possible mechanisms, it has been demonstrated that endostatin, via its affinity for heparan, binds to heparan sulfate proteoglycan (HSP) receptors on the endothelial cell surface, in competition with the TAF basic fibroblast growth factor (bFGF), although these binding sites can act as co-receptors for several cytokines (Sasaki et al. 1999). These same authors postulate that the same competitive process occurs in tumor-induced angiogenesis, although endostatin appears to have several other potential mechanisms of action (Mundehenke et al. 2001). These includes some evidence for action downstream of any TAF receptors on endothelial cells, most notably receptors for VEGF as well as bFGF and, inhibiting phosphorylation of extracellular signal-regulated kinases that activate these TAFs (Sim et al. 2000; Rehn et al. 2001), and thus angiogenesis. Nevertheless, its heparan sulfate binding domain appears prominently and recent indirect evidence has also demonstrated tumor suppression in mouse lung, skin, and prostate cancers following treatment with heparan sulfate (Mundehenke et al. 2001; Liu et al. 2002), the same group also suggesting that adding heparan or heparan sulfate to endostatin might enhance its anti-angiogenic, tumor suppressive effects.

We test this hypothesis in numero here, also expanding it to include other anti-angiogenic substances that either directly or indirectly inhibit proliferation of endothelial cells. A mathematical model of extratumoral angiogenesis is developed using the non-proliferative partial differential equation (PDE) model of Anderson and Chaplain (1998) as a starting point, augmented to include the dynamics of endothelial cell proliferation and postulated endostatin inhibition effects. Following their approach, the PDEs in the new model are discretized, and a biased random walk algorithm is incorporated to simulate the dynamics of endothelial cell proliferation and blood vessel branching in response to the drug. This is done for a wide range of endostatin and angiostatin clearance rates and typical reported dosage regimens, to gain insights into treatment efficacies and drug dynamics, as well as anti-angiogenic effects of endostatin and similarly suppressive anti-angiogenic drugs, as a function of these treatment parameters.

Methods

The continuous PDE model of Anderson and Chaplain (Anderson and Chaplain 1998)

This model depicts angiogenesis, as outlined above, implemented with partial differential equations to approximate the spatiotemporal changes in the concentration of the various substances

involved and the resulting angiogenic dynamics. The simulation space is a 200×200 rectilinear grid, assumed to represent a small portion of the anatomy where tumor-induced angiogenesis is being observed. Anderson and Chaplain (Anderson and Chaplain 1998) used data derived from experimental preparations of Gimbrone et al. (1974) and Muthukkaruppan et al. (1982) to quantify their model. The data was collected for a solid tumor, or fragment of tumor implanted in the mouse cornea close to the limbal vessels of the eye, which are lined with endothelial cells, and observations were made on the migratory behavior of endothelial cells and morphology of the blood vessel as a result of tumor-induced angiogenesis. New model development begins with an expanded explanation of Anderson and Chaplain's model, followed by discussion of the modifications.

Let $E(x,y,t) \equiv E$ (in Molarity, M) denote the time- and space-dependent concentration of endothelial cells, $T(x,y,t) \equiv T$ (M) the concentration of (lumped) TAFs, and $F(x,y,t) \equiv F$ (M) the concentration of Fn. These variables and other nomenclature used in this paper are given in Table 1. The generalized equations are:

$$\frac{\partial E}{\partial t} = D_E(E,T,F) + P_E(E,T,F) \quad (1)$$

$$\frac{\partial T}{\partial t} = D_T(E,T,F) + P_T(E,T,F) + S_T(E,T,F) \quad (2)$$

$$\frac{\partial F}{\partial t} = D_F(E,T,F) + P_F(E,T,F) + S_F(E,T,F) \quad (3)$$

where D_E, D_T and D_F are functions depicting the diffusion characteristics of endothelial cells, TAFs and Fn respectively; P_E, P_T and P_F are net production/loss terms, and S_T and S_F are functions representing uptake of substances by endothelial cells. To specify these terms, the authors assumed classic Fickian diffusion, with no net production/death of endothelial cells; linear uptake, production/loss rates for each substance; and a specific nonlinear response of endothelial cells to chemotaxis of TAF.

For diffusion of endothelial cells E, $D_E(E;T;F) = \bar{\nabla} J_E$, where J_E, the flux of endothelial cells, has three components: flux $J_{rand} = -a_e \bar{\nabla} E$, where a_e is a positive random motility coefficient; $J_{chemo} = a_c(T) E \bar{\nabla} T$, where $a_c(T) = \frac{a_c k}{k+T}$ (Lauffenberger and Kennedy 1984; Olsen et al. 1997; Anderson and Chaplain 1998), a_c is the saturable chemotaxis coefficient and k is a positive constant; and $J_{hapto} = a_h E \bar{\nabla} F$, where a_h is the haptotaxis constant. Therefore, endothelial cell flux is: $J_E = -a_e \nabla E + a_c(T) E \nabla T + a_h E \nabla F$. They assumed: (a) Fn production is linearly proportional to endothelial cell concentration; (b) the rate of Fn uptake by endothelial cells depends on the probability of contact between Fn and endothelial cells E, i.e., $uptake(F) = -b_u EF$, where b_u is the rate constant for Fn uptake by endothelial cells; and (c) uptake kinetics of TAF is similarly probabilistic, $uptake(T) = -c_u ET$, where c_u is the rate constant for

Table 1 Nomenclature & parameter values from: (Anderson and Chaplain 1998; Carmeliet and Collen 1997; Folkman 1997; Molema et al. 2001; Orme and Chaplain 1997; Sharma and Jusko 1998) and Appendix

Symbol	Description	Value	Units
E	Concentration of unbound endothelial cells at (x,y,t)	Variable	M (Molarity)
T	TAF concentration at (x,y,t)	Variable	M
F	Fibronectin concentration at (x,y,t)	Variable	M
T^*	TAF concentration threshold	8.477×10^{-12}	M
E_0	Initial concentration of endothelial cells at the parent vessel.	1×10^{-10}	M
F_0	Initial concentration of Fn at the parent vessel	1×10^{-10}	M
T_0	Initial concentration of TAF at the parent vessel	4.2385×10^{-11}	M
I	Endostatin concentration	Variable	M
$\epsilon_{\max}$	Inhibition coefficient	1	Dimensionless
IC_{50}	Half-maximal inhibition concentration	2.288×10^{-8}	M
I_0	Initial concentration of endostatin at the parent vessel	1.99×10^{-9}	M
I_{ex}	Exogenously introduced endostatin concentration	Variable	M
I_{en}	Endogenous endostatin concentration	Variable	M
$U_{I,en}$	Endogenous endostatin input	Variable	g/s
$U_{I,ex}$	Exogenous inputs of endostatin	20 and 200	$mg/kg/day$
$\bar{V}$	Gradient function $(\partial/\partial x, \partial/\partial \gamma, \partial/\partial z)$	Variable	cm^{-1}
J_E	Total flux of endothelial cells	Variable	$cm \times M/s$
J_{rand}	Flux of endothelial cells due to simple diffusion	Variable	$cm \times M/s$
J_{chemo}	Flux of endothelial cells due to TAF gradient	Variable	$cm \times M/s$
J_{hapto}	Flux of endothelial cells due to Fn gradient	Variable	$cm \times M/s$
α_e	Endothelial cell diffusion coefficient	10^{-10}	cm^2/s
α_h	Haptotaxis coefficient	0.00075	$cm^2/(s \times M)$
$\alpha_c(T)$	Chemotaxis function	Variable	$cm^2/(s \times M)$
α_c	Chemotaxis coefficient	2600	$cm^2/(s \times M)$
α_r	Endothelial cell proliferation rate	5.56×10^{-5} to 1.556×10^{-4}	$1/s$
α_d	Endothelial cell loss rate	5.56×10^{-6} to 1.556×10^{-5}	$1/h$
b_p	Fn production rate	3.625×10^{-7}	$1/s$
b_u	Fn rate of uptake by endothelial cells	725	$1/(s \times M)$
c_u	TAF rate of uptake by endothelial cells	725	$1/(s \times M)$
t_c	TAF diffusion coefficient	2.9×10^{-7}	cm^2/s
t_d	Distance between parent vessel to tumor	0.2	cm
V_p	Plasma volume	10^{-3}	L
Cl_I	Simulated clearance range	0.3×10^{-5} to 10^{-4}	L/s
	Endostatin clearance[a]	5.54×10^{-5}	L/s
	Angiostatin clearance[b]	2.56×10^{-5}	L/s
β,ξ,ϕ,γ	Normalized variables	Derived values	Dimensionless

[a]To our knowledge, the endostatin plasma clearance rate-C_I has been reported only for the human, as 22.6 ($l \cdot h \cdot m^2$) (Thomas et al. 2000). After unit conversion and allometric scaling between mouse and human, with allometric exponent 0.74 (Hu et al. 2001), endostatin clearance in the 20 g mouse is estimated as: $Cl_I^{mouse} = 22.6(\frac{L}{hr \cdot m^2})\frac{1}{3600}(\frac{hr}{s})1.7m^2(\frac{20g}{70000g})^{0.74} = 5.54 \cdot 10^{-5}(\frac{L}{s})$ [b]Angiostatin clearance in the rat has been reported as 0.128 ml/min (Molema et al. 2001). This has been scaled, as above, for the 20 g mouse as: $Cl_I^{mouse} = 0.128(\frac{ml}{\min})\frac{1}{60}(\frac{\min}{s})\frac{1}{1000}(\frac{L}{ml})(\frac{20g}{200g})^{0.74} = 1.17 \cdot 10^{-5}(\frac{L}{s})$ We used an eightfold range including these two values for endogenous drug administration simulations

TAF uptake by endothelial cells. The model was further simplified by assuming: (d) very slow turnover of cells E, and thus the net production/death term for endothelial cells $P_E = 0$ in Eq. (1). They also assumed: (e) diffusion of Fn is minimal; and (f): P_T D_T and D_F are zero in Eqs. (2) and (3), because TAFs have very rapid diffusion rates, and achieve a pseudo-steady state approximately instantaneously relative to other processes in Eq. (2).

The Anderson-Chaplain model (1), with $P_E \equiv D_F \equiv D_T \equiv 0$, thus becomes:

$$\begin{aligned}\frac{\partial E}{\partial t} = D_E = \nabla[-J_E] = \nabla\left[-J_{chemo} - J_{hapto} - J_{rand}\right] \\ = \nabla[-a_c(T)E\nabla T - a_h E\nabla F + a_e\nabla E]\end{aligned} \tag{4}$$

$$\frac{\partial T}{\partial t} = S_T = -c_u ET \tag{5}$$

$$\frac{\partial F}{\partial t} = P_F + S_F = b_p E - b_u EF \tag{6}$$

New model

Anderson and Chaplain (Anderson and Chaplain 1998) assumed that endothelial cells did not proliferate over the time course of application of their continuous model [(d) above], justified by endothelial cells having a half-life on the order of months. Although this assumption may be valid under normal physiological conditions, the proliferation mechanisms during tumor-induced angiogenesis and during drug treatment probably have different dynamics, e.g., the presumed inhibitory effects of endostatin on endothelial cell proliferation. Thus, we reintroduce proliferation and death of endothelial cells for describing tumor-induced angiogenesis and treatment, based on an earlier model of the dynamics of endothelial cell populations (Chaplain and Stuart 1993).

Endothelial cell proliferation due to mitogenic stimulation alone

Mitogen-stimulated proliferation begins with binding of a mitogen particle with a surface receptor on the endothelial cell (Carmeliet and Collen 1997). Once bound, the surface receptor transduces this signal, from the cell membrane to intracellular mechanisms responsible for growth, and it thereby activates cell growth. The activated endothelial cells then proceed onto the next phase of the cell cycle and eventually undergo mitosis. On a cell population level, we adopt Chaplain and Stuart's (Chaplain and Stuart 1993) formulation to describe an endothelial cell population proliferating at any fixed point in space (x', y'). The authors assumed that mitosis is governed by logistic type growth, with cell loss a first-order process:

$$\frac{\partial E}{\partial t} = a_r\left(1 - \frac{E}{E_0}\right)EG(T) - a_d E \tag{7}$$

where a_r is a positive constant related to the maximum mitosis rate, a_d is the rate constant for endothelial cell loss, $E = E(x', y')$, E_0 is the initial concentration of E at the parent vessel, and TAF exerts a threshold concentration effect on endothelial cell growth, represented as:

$$G(T) = \begin{cases} 0 & \text{if } T \leqslant T^* \\ (T - T^*)/T_0 & \text{if } T^* < T \end{cases} \tag{8}$$

In Eq. (8), T^* is the TAF concentration threshold and T_0 is the TAF concentration at the tumor cluster boundary.

Proliferation due to mitogenic stimulation plus inhibition of mitogenesis by endostatin

We assume a simple linear model for plasma endostatin kinetics, $V_p\frac{\partial I}{\partial t} = U - Cl_I I$, where I is the plasma concentration of endostatin, $V_p(L)$ is the plasma volume, $Cl_I(L/s)$ is the endostatin plasma clearance rate, and $U = U_{I,en} + U_{Iex}(M/s)$ is the endostatin endogenous plus exogenous production rates. For adequate exogenous doses, $U_{I,ex} \gg U_{I,en}$ (Thomas et al. 2000) and the endostatin equation simplifies further to:

$$\frac{\partial I}{\partial t} = \left(-Cl_I I + U_{I,ex}\right)/V_p \tag{9}$$

Coupling of I with E is accomplished as follows: we assume endostatin exerts its anti-angiogenic effect by inhibiting any of several possible pathways. These include inhibition of mitogen-stimulated proliferation or migration of endothelial cells, either through competition with TAFs for binding with HSP receptors on the endothelial cell surface, and not by sequestration in the extracellular matrix — which is also possible (Sasaki et al. 1999), or by action downstream of any TAF receptors, most notably receptors for bFGF and VEGF, possibly inhibiting phosphorylation of extracellular signal-regulated kinases that activate these TAFs (Sim et al. 2000), and thus angiogenesis. The indirect inhibition function of Sharma and Jusko (1998) is sufficiently robust to describe any of these possible inhibitory effects:

$$Inhibition(t) = 1 - \frac{\varepsilon_{\max} I}{IC_{50} + I},\ 0 \leqslant \varepsilon_{\max} \leqslant 1 \tag{10}$$

is the maximum fractional ability of endostatin to affect endothelial cell proliferation, and IC_{50} is the endostatin concentration that induces 50% maximum inhibition at the effect site. If the hypothesis is correct, this function affects growth, the first term in Eq. (7), as a multiplicative factor. Thus, augmenting Eq. (4) with (7) and (10), we get Eq. (11):

$$\begin{aligned}\frac{\partial E}{\partial t} = \nabla[-a_c(T)E\nabla T - a_h E\nabla F + a_e\nabla E] \\ + a_r\left(1 - \frac{E}{E_0}\right)EG(T)\left(1 - \frac{\varepsilon_{\max} I}{IC_{50} + I}\right) - a_d E\end{aligned} \tag{11}$$

with G in (11) defined by Eq. (8). Equations (5), (6), and (9) complete the four-PDE model.

As in (1), we normalize these PDEs by rescaling time: $\tau = t_d^2/t_c$. Here t_d is the parent-vessel-to-tumor distance and t_c is the TAF diffusion coefficient, and the dependent variable concentrations by their initial concentrations, T_0, F_0 and E_0: $\overline{T} = \frac{T}{T_0}$, $\overline{F} = \frac{F}{F_0}$, $\overline{E} = \frac{E}{E_0}$, $\bar{t} = \frac{t}{\tau}$ and $\overline{I} = \frac{I}{I_0}$. Making the above conversions and removing the bar above each symbol for clarity, the four normalized PDEs become:

$$\begin{aligned}\frac{\partial E}{\partial t} = \nabla[-\beta_c(T)E\nabla T - \beta_h E\nabla F + \beta_e\nabla E] \\ + \beta_r(1 - E)EG(T)\left(1 - \frac{\varepsilon_{\max} I_0 I}{IC_{50} + I_0 I}\right) - \beta_d E\end{aligned} \tag{12}$$

$$\frac{\partial F}{\partial t} = \xi_p E - \xi_u EF \tag{13}$$

$$\frac{\partial T}{\partial t} = -\varphi_u ET \tag{14}$$

$$\frac{\partial I}{\partial t} = -\gamma_c I + \gamma_u U_{I,ex} \tag{15}$$

where $\beta_c(T) = \frac{\beta_{c1}}{1+\beta_{c2}T}$, $\beta_{c1} = \frac{a_c T_0}{t_c}$, $\beta_{c2} = \frac{T_0}{k}$, $\beta_e = \frac{a_e}{t_c}$, $\beta_h = \frac{a_h F_0}{t_c}$, $\xi_p = \frac{b_p t_d^2 E_0}{F_0 t_c}$, $\xi_u = \frac{b_u t_d^2 E_0}{t_c}$, $\varphi_u = \frac{c_u t_d^2 E_0}{t_c}$, $\beta_r = \frac{t_d^2 r}{t_c}$, $\beta_d = \frac{t_d^2 a_d}{t_c}$, $\gamma_c = \frac{Cl_I t_d^2}{t_c v_p}$, $\gamma_u = \frac{t_d^2}{t_c I_0 v_p}$ and

$$G(T) = \begin{cases} 0 & \text{if} T \leqslant T^* \\ T - T^* & \text{if} T^* < T \end{cases} \tag{16}$$

Table 1 includes the complete nomenclature and parameter values.

Results

Simulation conditions

We used Euler's finite difference approximation to discretize the continuous PDEs for simulation, as in

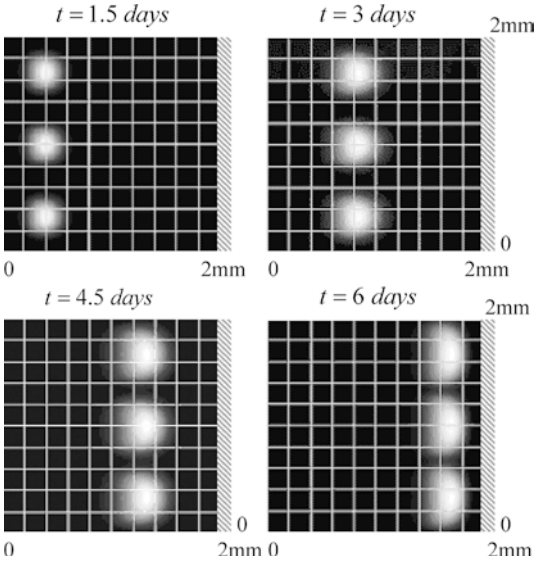

Fig. 1 Spatiotemporal evolution of three *endothelial cell clusters migrating* toward a *linear tumor*, shown as a cross-hatched region beginning at x = 2 mm and extending from y = 0 to y = 2 mm, simulated without haptotaxis, proliferation or degradation of endothelial cells. The x-y ranges are 0–2 mm in all graphs, representing a distance of 2 mm between the parent vessel (at x = 0) and tumor (at x = 2 mm), with tumor producing TAF along the whole of x = 2 mm. For cells with diameter about 20 microns, each cluster has about 10 cells at x = 0. The highest density clusters dominate the graphs, as *bright white* growing objects. Lower density clusters, not shown, follow behind these

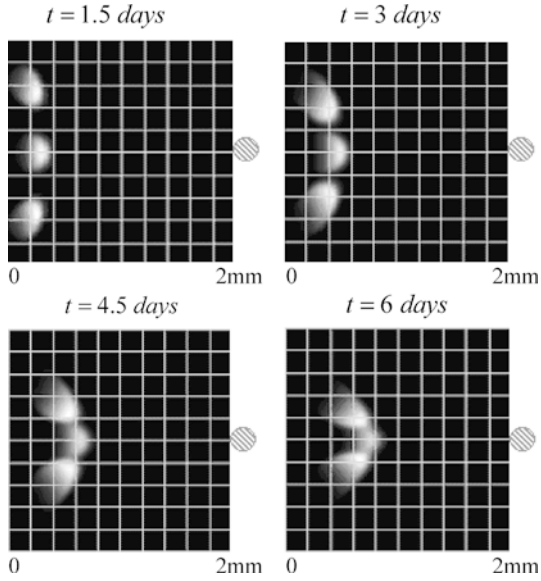

Fig. 2 Spatiotemporal evolution of three *endothelial cell clusters,* as in Fig. 1, but migrating toward a *0.2 mm diameter circular tumor*, in this case with both haptotaxis and chemotaxis, but without proliferation or degradation. Eventually the growing clusters reached the tumor

Anderson and Chaplain (1998). Details are given in the Appendix for both the discretization and the biased random-walk model of vessel growth used in the simulations. In all results shown below, simulations begin after TAF has diffused across the extracellular space and reached the neighboring blood vessels, with three initial clusters of endothelial cells, positioned at x = 0 on the square simulation space graphs, formed in response to TAF stimulation. The tumor cells are positioned at $x = 0.2$ mm, the distance from parent vessel to tumor, with x–y ranges from 0 mm to 0.2 mm in all figures. The initial concentration distributions of TAF and Fn are described by exponentially decaying functions, as given in Anderson and Chaplain (Anderson and Chaplain 1998). In their model and in ours, 2 s of scaled model time are equivalent to 3 days real time. We express time as *real* time, in days, in all figures.

We validated our model augmentations by reproducing results reported in the reference, using the same parameter values to test our model under the same conditions (see Table 1). We first simulated spatiotemporal evolution of endothelial cell concentrations from the parent vessel toward the linearly arranged tumor, without haptotaxis. Thus, $\beta = 0.00035$, $\beta_{c2} = 0.6$, $\beta_{c2} = 0.38$, $\beta_h = 0.34$, $\beta_r = 0$, $\beta_d = 0$, $\xi_p = 0.05$, $\xi_u = 0.1$, $\phi_u = 0.1$, $\gamma_u = 0.1$, $\gamma_c = 0$, $h = 0.005$, and k = 1,000. Our results, shown in Fig. 1, illustrate the wavefront of three cell clusters moving parallel to each other, reaching the tumor at about $t = 6$ days real time, as in Anderson and Chaplain (Anderson and Chaplain 1998). The brightest white in this and other figures represents the highest density of cells, with lower densities to the left hardly apparent.

We also simulated the migration of endothelial cells in the presence of Fn (not shown), which was slower than without Fn; lateral cell movement was more pronounced, causing the cell clusters to spread vertically, all as in Anderson and Chaplain (Anderson and Chaplain 1998). Vertical cluster spreading was more apparent than in Fig. 1. Eventually the clusters joined to form a continuous horizontal band. We then simulated the growth of blood vessels without the influence of Fn (not shown), clearly demonstrating that the trees of blood vessels are drawn toward the linear array of tumors located at $x = 1$ of the model space. Initial growth of blood vessels (from $t = 0$ to $t = 1.5$ days) had trees of vessels extending parallel to each other. Due to the inherent stochastic nature of the biased random-walk component of the model, the top two vessel trees are drawn toward each other. This result is comparable to that in Anderson and Chaplain (Anderson and Chaplain 1998); blood vessels still migrated rapidly toward the tumors.

Under the influence of Fn, lateral extension of blood vessels was more pronounced (not shown), corresponding directly to an increased rate of branching. In addition, as early as $t = 10$–1/2 days real time, the network of blood vessels formed a so-called brush-border. This phenomenon has been observed in vitro (Muthukkaruppan et al. 1982).

In contrast, cell migration with the *circular tumor* had different kinetics, shown at 1–1/2 days, 3 days, 4–1/

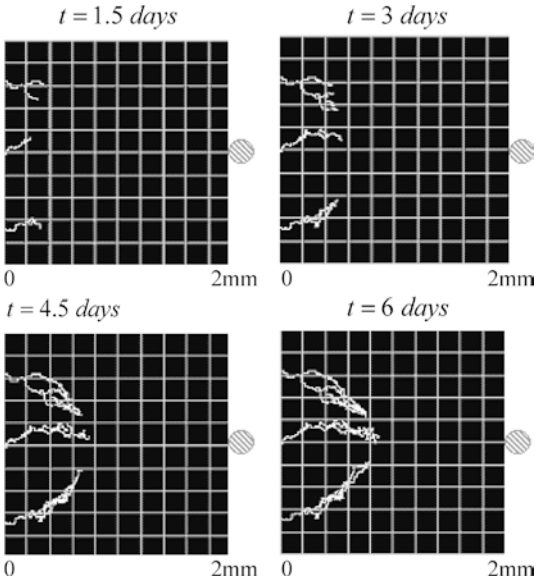

Fig. 3 Spatiotemporal evolution of *vessel growth* toward a *single 0.2 mm diameter circular tumor*, with both haptotaxis and chemotaxis, but without proliferation or degradation of endothelial cells. Eventually the vessels reached the tumor

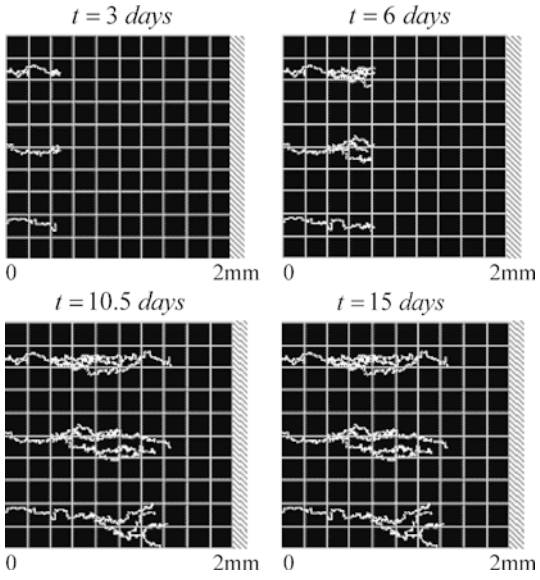

Fig. 4 Spatiotemporal evolution of *vessel growth* toward a *linear tumor*, extending from y = 0 to y = 2 mm at x = 2 mm, as in Fig. 1, with haptotaxis, chemotaxis, proliferation, and degradation of endothelial cells all included

2 days, and 6 days in Fig. 2, with both chemotaxis and haptotaxis present. The cell clusters converged toward the tumor located at the midline of the model space, eventually reaching the tumor, as in Anderson and Chaplain (Anderson and Chaplain 1998). Figure 3 depicts blood vessel growth in the presence of a single circular tumor cluster located on the model space graph as shown. The blood vessel growth pattern in Fig. 3 exhibits convergence toward the circular tumor, also as in Anderson and Chaplain (Anderson and Chaplain 1998).

Simulation including endothelial cell proliferation and degradation mechanisms

From Table 1, we use the additional parameter values: $\alpha_r = 5.56\times10^{-5}$ and $\alpha_d = 5.56\times10^{-6}$ to include this model extension. Migration of endothelial cells (not shown) and blood vessel growth shown from 3 days to 15 days in Fig. 4 are as in Anderson and Chaplain (Anderson and Chaplain 1998).

Exogenous endostatin and angiostatin dosing simulations

We simulated single bolus injections of 20 mg·kg·day and 200 mg·kg·day, and constant infusions of 20 mg·kg·day and 200 mg·kg·day for 20 simulated days. In these first drug response runs, we used the reported human endostatin clearance rate, scaled for the mouse (see Table 1), $Cl_I = 5.54\times10^{-5}$ l/s. Neither bolus dosage was predictively capable of arresting vessel growth or cell migration (Fig. 5 and Fig. 6). In contrast, Fig. 7 shows

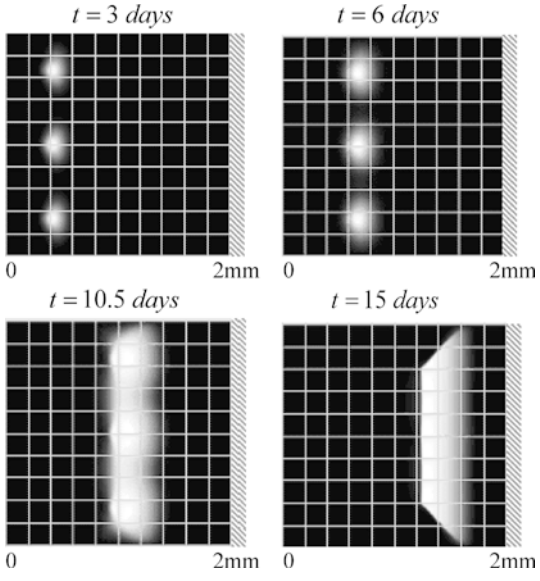

Fig. 5 Spatiotemporal evolution of three *endothelial cell clusters* migrating toward the same linear tumor as in Fig. 4, with haptotaxis, chemotaxis, proliferation, and degradation of endothelial cells all included, and an *endostatin bolus* injection of *200 mg*·kg·day. Eventually the clusters reached the tumor

that constant infusions stop vessel growth at $t = 3$ days real time, even for the lower 20 mg·kg·day dose.

We repeated the above simulations over an eightfold range of drug clearance rates, 0.3×10^{-5} to 10^{-4} l/s, which include the scaled values for endostatin, and also for angiostatin clearances (see Table 1), assuming that angiostatin might act via a quantitatively similar mechanism, directly or indirectly, e.g., via a pathway mechanism that ultimately inhibits or blocks endothelial

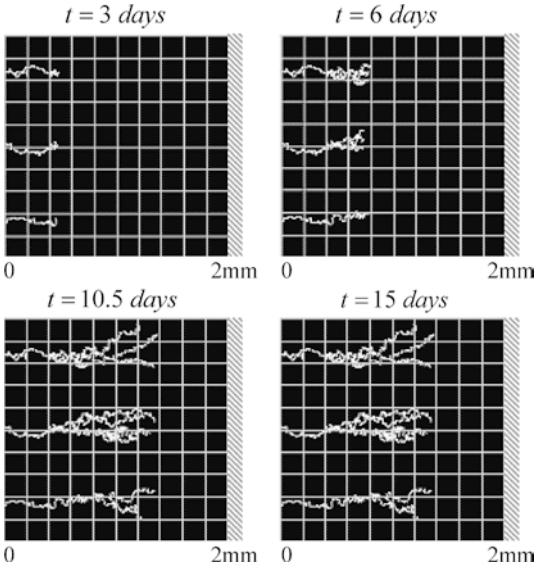

Fig. 6 Spatiotemporal evolution of vessel growth toward the same linear tumor as in Fig. 4, with haptotaxis, chemotaxis, proliferation, and degradation of endothelial cells, and an *endostatin bolus* injection of *200 mg*·kg·day. Eventually the vessels reached the tumor

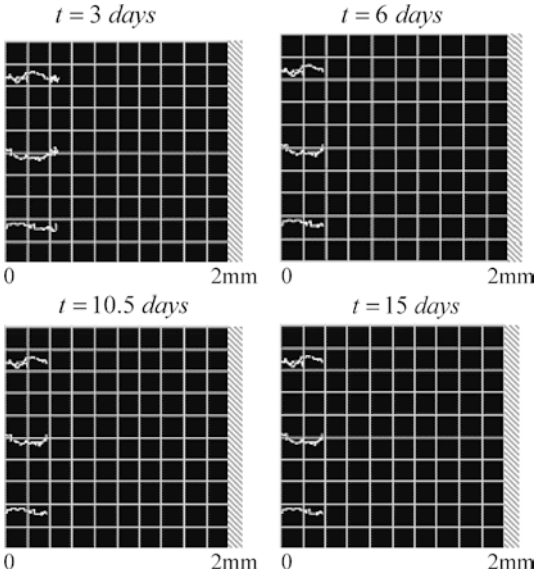

Fig. 7 Spatiotemporal evolution of vessel growth toward the same linear tumor as in Fig. 4, with haptotaxis, chemotaxis, proliferation, and degradation of endothelial cells and an *endostatin infusion of 20 mg*·kg·day. Vessel growth ceased at $t = 3$ days real time. In this simulation, clearance was the scaled measured value for endostatin, 5.54×10^{-5} l/s

cell proliferation. For this range, neither bolus dose arrested angiogenesis over the same simulation interval. In contrast, all simulations with constant infusion inputs of drug arrested vessel growth at $t = 3$ days real time, even with the lower dose. This is illustrated for the largest clearance rate and lowest dosage in Fig. 8. For clearance rates greater than this range (not shown), neither constant infusion nor the bolus dose inputs were

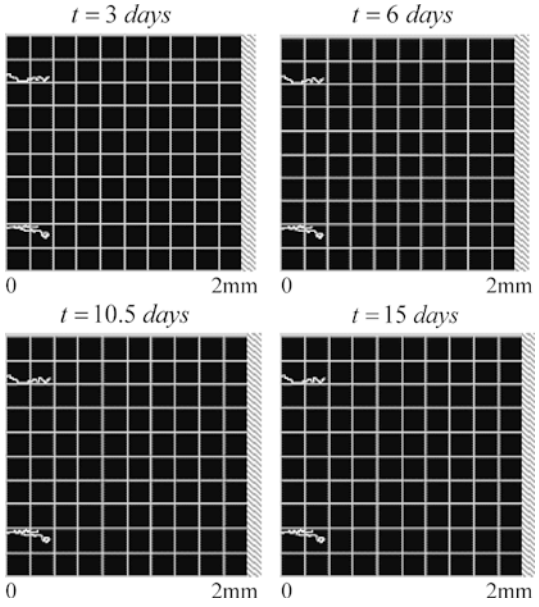

Fig. 8 Spatiotemporal evolution of vessel growth toward the same linear tumor as in Fig. 4, with haptotaxis, chemotaxis, proliferation, and degradation of endothelial cells, and an *endostatin infusion of 20 mg*·kg·day. In this case, the max of the range of clearances tested, 10^{-4} l/s, was used. Again, vessel growth ceased at 3 days real time

predictively capable of stopping vessel growth over the 20 days of simulated inputs.

Discussion

Drug dynamics in vivo are generally governed by mathematically nonlinear processes, most commonly receptor or other mass action-based interactions and, among other things, this means that the manner in which a drug is introduced can influence its effectiveness in vivo. Certainly, if the rate of elimination of the drug is so rapid that it does not remain at the active site long enough, or in sufficient concentration, it will not have its desired effect; but fabricating the drug so that its clearance rate is reduced may or may not overcome this problem, depending on its mechanism of action and possibly other complicating factors. When the mechanism is nonlinear, the dynamic response of the drug-host system is dependent on the shape as well as the magnitude of the (exogenous drug) input, a well-known property of nonlinear systems. This seems to be the case for the nonlinear anti-angiogenesis model considered here: presumably equipotent inputs of different shape over time, i.e., repeated pulse-dose versus constant infusion inputs, with equal integrals (or AUCs), generate different simulated biosystem responses, one effective the other not.

In our analysis, we first showed that simulation results obtained with our new model, which incorporates additional terms depicting (nonlinear) proliferation and (linear) degradation of endothelial cells, are consistent

with corresponding results in Anderson and Chaplain (Anderson and Chaplain 1998). We augmented the model in this manner to make it more realistic for representing pathologies. We also incorporated a nonlinear indirect inhibition function (Sharma and Jusko 1998), for representing the effects of endostatin and similarly acting TAF inhibitors on growth of endothelial cells and the dynamics of angiogenesis during anti-angiogenic drug treatment. We simulated two dosing patterns for endostatin as input to our model: bolus injection and constant infusion. For each one, we simulated responses for two drug dosage levels, single daily or 20-day infusions of 20 mg·kg·body weight (BW), the dosage of choice in most preclinical studies (Sim et al. (2000), or a tenfold greater simulated dose: 200 mg·kg·BW.

Simulated constant infusion of endostatin predictively yielded more promising results: blood vessels stopped growing as early as $t = 3$ days real time. We reproduced this result with two different endostatin infusion rates, strongly suggesting that the consistent inhibition predicted by simulation is not due to chance associated with the stochastic nature of the model, and a tenfold greater (200) than typical dosage (20) was not enough to overcome the deficiency of the pulse-dosing pattern**.** Indeed, our results are also consistent with real data on angiostatin dosing patterns in mice, where continuous infusion of the drug had a dramatically improved anti-angiogenic effect over even twice daily administration of the same dose, from 1 mg·kg·day up to 100 mg·kg·day (Drixler et al. 2000). In these same studies, constant infusion of 100 mg·kg·day resulted in significantly greater inhibition of the growth of primary and metastatic tumors, lending support to use of constant infusion rather than pulse-dose drug inputs for both anti-angiogenic and tumoricidal effects (Sim et al. 2000).

Recent results by McDougall et al. (McDougall et al. 2002) lend further support to our results, as well as a possible biophysical explanation for the efficacy of constant over pulsed inputs. This group simulated the dynamics of distributed flow of an arbitrary chemotherapeutic drug in a newly generated vascular network following angiogenesis of a tumor. This 2-D model predicts that the drug rapidly bypasses the tumor region following IV *bolus* drug administration, diluted by fresh blood following passage of the bolus within the larger network of already diluting flow pathways. In contrast, the flow dynamics following IV *continuous infusion* resulted in persistence of the drug in the blood vessels adjacent to the tumor, a proximity presumably necessary for anti-angiogenic or other therapeutic action.

We also explored the effectiveness of endostatin therapy as a function of its plasma clearance rate, by varying the clearance rate over an eightfold range, which included the value for endostatin clearance, scaled from human kinetic data. The angiostatin clearance rate reported for rat and scaled to mouse also is included in this range, and therefore our results should apply for angiostatin, if its mechanism of action is similarly modeled, even via a specifically different mechanism than that of endostatin (Sim et al. 2000), but with equations also depicting direct or indirect inhibition of endothelial cell proliferation, as in Eqs. (10) and (11). In this sense, the way we have implemented inhibition of TAFs by endostatin in our model is robust. It may be a reasonable way of implementing direct or indirect effects of other candidates in the growing list of pro-angiogenic factors, including those involved in suppressing the effects of the bFGFs and VEGFs (Novak 2002a) as well as others.

We hasten to point out that, at the time of anti-angiogenic drug treatment, our model represents treatment of continuing extratumoral angiogenesis of established tumors, which typically have a fairly well-developed blood supply, with vessels penetrating the tumors to various depths. For a more precise understanding of tumor angiogenesis in all its stages, it will be of interest to extend our model to include intratumoral vasculature dynamics, including pressure effects, vessel degradation, and temporal variations in blood flow due to transient vascular occlusion or spasm, among other processes.

In conclusion, our new model predicts that constant infusion of endostatin and similarly acting agents is more effective therapeutically on inhibiting or arresting extratumoral angiogenesis than are equipotent bolus injections, at least in the mouse, over an eightfold range of clearance rates of the drug. Nevertheless, clearance rates still matter, as neither dosing pattern was effective for clearance rates greater than about 10^{-4} l/s in the mouse model.

Appendix: Discretization of the augmented continuous PDEs and the biased random walk model of vessel growth

We use Euler's finite difference approximation to discretize the continuous PDE for simulation, as in Anderson and Chaplain (Anderson and Chaplain 1998). The gradient vector operator $\bar{\nabla}$, expressed in terms of the two space variables, x and y, is

$$\nabla = i\frac{\partial}{\partial x} + j\frac{\partial}{\partial y} \tag{A1}$$

where i and j are vectors in the x and y directions respectively. Expanding Eq. (12) using (A1) gives:

$$\begin{aligned}\frac{\partial E}{\partial t} = {} & \beta_e\left(\frac{\partial^2 E}{\partial x^2} + \frac{\partial^2 E}{\partial y^2}\right) - \frac{\partial}{\partial x}\left(\beta_c(T)E\frac{\partial T}{\partial x}\right) - \frac{\partial}{\partial y}\left(\beta_c(T)E\frac{\partial T}{\partial y}\right) \\ & - \frac{\partial}{\partial x}\left(\beta_h E\frac{\partial F}{\partial x}\right) - \frac{\partial}{\partial y}\left(\beta_h E\frac{\partial F}{\partial y}\right) \\ & - \beta_r E(1-E)G(T)\left(1 - \frac{\varepsilon_{\max} I_0 I}{IC_{50} + I_0 I}\right) - \beta_d E\end{aligned} \tag{A2}$$

The simulation space is discretized by setting $x = hl$, $y = hm$ and time $t = kq$, where h is the fractional grid step and k is the fractional time step. The first and second derivatives are approximated using the following explicit Euler scheme:

$$\frac{\partial v[q+1]}{\partial t} = \frac{v[q+1]-v[q]}{k} \tag{A3}$$

$$\frac{\partial v[l,m]}{\partial x} = \frac{v[l+1,m]-v[l-1,m]}{2h} \tag{A4}$$

$$\frac{\partial v[l,m]}{\partial y} = \frac{v[l,m+1]-v[l,m-1]}{2h} \tag{A5}$$

$$\frac{\partial^2 v[l,m]}{\partial x^2} = \frac{v[l+1,m]-2v[l,m]+v[l-1,m]}{h^2} \tag{A6}$$

$$\frac{\partial^2 v[l,m]}{\partial y^2} = \frac{v[l,m+1]-2v[l,m]+v[l,m-1]}{h^2} \tag{A7}$$

Equations (A3)–(A7) substituted into Eq. (A2) and Eqs. (13)–(16) provide the discretized version for simulation. However, we additionally augment these recursive equations with stochastic behavior, by introducing the biased random walk parameters A_0, A_1, ..., A_4 for predicting endothelial cell migration behavior, as in Anderson and Chaplain (Anderson and Chaplain 1998). This gives:

$$\begin{aligned} E[l,m,q+1] &= A_0E[l,m,q]+A_1E[l+1,m,q]+A_2E[l-1,m,q] \\ &+A_3E[l,m+1,q]+A_4E[l,m-1,q] \\ &+k\beta_r E[l,m,q](1-E[l,m,q])G(T[l,m,q]) \\ &(1-\frac{I_{\max}I_0I[l,m,q]}{IC_{50}+I_0I[l,m,q]})-k\beta_d E[l,m,q] \end{aligned} \tag{A8}$$

$$\begin{aligned} F[l,m,q+1] &= F[l,m,q](1-k\xi_u F[l,m,q]) \\ &+k\xi_p E[l,m,q] \end{aligned} \tag{A9}$$

$$T[l,m,q+1] = T[l,m,q](1+k\varphi_u E[l,m,q]-k\mathrm{K}_1 E[l,m,q]) \tag{A10}$$

$$I[l,m,q+1] = (1-k\gamma_c)I[l,m,q]+k\gamma_u U_{I,ex} \tag{A11}$$

where the probability functions describing endothelial cell migratory behavior are:

$$\begin{aligned} A_0 &= 1-\tfrac{4k\beta_n}{h^2}+\tfrac{k\beta_{c2}\beta_c[T[l,m,q]]}{4h^2(1+\beta_{c2}T[l,m,q])}\left(\left(T[l+1,m,q]-T[l-1,m]\right)^2+\left(T[l,m+1,q]-T[l,m-1,q]\right)^2\right) \\ &-\tfrac{k\beta_c[T[l,m,q]]}{h^2}(T[l+1,m,q]+T[l-1,m,q]+T[l,m+1,q]+T[l,m-1,q]-4T[l,m,q]) \\ &-\tfrac{k\beta_h}{h^2}(F[l+1,m,q]+F[l-1,m,q]+F[l,m+1,q]+F[l,m-1,q]-4F[l,m,q]) \\ A_1 &= \tfrac{k\beta_n}{h^2}-\tfrac{k}{4h^2}(\beta_c[T[l,m,q]](T[l+1,m,q]-T[l-1,m,q])+\beta_h(F[l+1,m,q]-F[l-1,m,q])), \\ A_2 &= \tfrac{k\beta_n}{h^2}+\tfrac{k}{4h^2}(\beta_c[T[l,m,q]](T[l+1,m,q]-T[l-1,m,q])+\beta_h(F[l+1,m,q]-F[l-1,m,q])), \\ A_3 &= \tfrac{k\beta_n}{h^2}-\tfrac{k}{4h^2}(\beta_c[T[l,m,q]](T[l,m+1,q]-T[l,m-1,q])+\beta_h(F[l,m+1,q]-F[l,m-1,q])), \\ A_4 &= \tfrac{k\beta_n}{h^2}+\tfrac{k}{4h^2}(\beta_c[T[l,m,q]](T[l,m+1,q]-T[l,m-1,q])+\beta_h(F[l,m+1,q]-F[l,m-1,q])). \end{aligned}$$

Specifically, A_0 is proportional to the probability of no movement; A_1, A_2, A_3, and A_4 are proportional to the probability of moving to the right, left, up and down respectively along the chosen grid. Given that blood vessel growth is influenced primarily by migration, branching and mitosis of endothelial cells, the rationale for this model is based on the following four assumptions (Anderson and Chaplain 1998): (a) The concentration of endothelial cells near the tip of a sprout must be adequate for lengthwise growth. (b) There must be enough space for lengthwise growth. (c) The direction of growth depends on the five probability functions noted above: $A_0 - A_4$. As in Anderson and Chaplain (1998), we construct five ranges: $R_0 = [0, A_1], R_j = [\sum_{i=0}^{j-1} A_i, \sum_{i=0}^{j} A_i, j = 1,2,3,4$. A random number is generated, and depending on the range in which this number falls, the direction of growth will change. If it falls in R_0, the sprout will remain stationary. However, if it falls in either R_1, R_2, R_3 or R_4, the current vessel branch will extend in either the right, left, up or down direction along the chosen grid. (d) Branching occurs only at the sprout tip, and only if: (i) the age of the sprout is greater than some threshold $\Gamma\alpha$; (ii) there is enough space for creation of new branch; (iii) the endothelial cell concentration at the branching site is high enough, $x_n \geqslant \Gamma_d$, and (iv) the probability of branching is proportional to the TAF concentration. A piecewise-continuous representation of the probability function was used in (1). In our augmented model, it was convenient to use a continuous probability function, with a similar shape: $P_b[x_c] = \frac{1}{1+\delta(x_c)^\sigma}$ with δ and σ as positive constants because its shape can be precisely controlled by adjusting its parameters, δ and σ. $P_{\mathrm{b,max}} = 1$ and $P_{b,\min} = \frac{1}{1+\delta}$, and its inflection point is controlled by σ.

References

Anderson ARA, Chaplain MAJ (1998) Continuous and discrete mathematical models of tumor-induced angiogenesis. Bull Math Biol 60:857–900

Carmeliet P, Collen D (1997) Molecular analysis of blood vessel formation and disease. Am J Physiol 273 [Heart Circ Physiol 42]:H2091-H2104

Chaplain MAJ, Stuart MA (1993) A model mechanism for the chemotaxis response of endothelial cells to tumor angiogenesis factor. IMA J Math Appl Med Biol 10:149–168

Drixler TA, Rinkes IH, Ritchie ED, van Vroonhoven TJ, Gebbink MF, Voest EE (2000) Continuous administration of angiostatin inhibits accelerated growth of colorectal liver metastases after partial hepatectomy. Cancer Res 60:1761–1765

Folkman J, Klagsbrun M (1987) Angiogenic factors. Science 235:442–447

Folkman J (1997) Endostatin: an endogenous inhibitor of angiogenesis and tumor growth. Cell 88:277–285

Gimbrone MA, Cotran RS, Leapman SB, Folkman J (1974) Tumor growth and neovascularization: an experimental model using the rabbit cornea. J Natl Cancer Inst 52:413–427

Griffioen AW, Molema G (2000) Angiogenesis: potentials for pharmacological intervention in the treatment of cancer, cardiovascular diseases and chronic inflammation. Pharmacol Rev 52:237–268

Ingber D (1990) Fn controls capillary endothelial cell growth by modulating cell shape. Proc Natl Acad Sci 87:3579–3583

Hu T-M, Hayton WL (2001). Allometric scaling of xenobiotic clearance: uncertainty versus universality. AAPS PharmSci 2000 3:1–14

Lauffenberger D, Aris R, Kennedy CR (1984) Travelling bands of chemotactic bacteria in the context of population growth. Bull Math Biol 46:19–40

Liu D, Shriver Z, Venkataraman G, El Shabrawo Y, Sasisekharan R (2002) Tumor cell surface heparan sulfate as cryptic promoters or inhibitors of tumor growth and metastasis. PNAS 99: 568–573

McDougal SR, Anderson ARA, Chaplain MAJ, Sheraratt JA (2002) Mathematical modelling of flow through vascular networks: implication for tumour-induced angiogenesis and chemotherapy strategies. Bull Math Biol 64:673–702

Molema G, Van Veen-Hof I, Van Loenen-Weemaes A, Proost JH, De Leu LFMH, Meijer DKF (2001) Pharmacokinetics and whole body distribution of elastase derived angiostatin (K1–3) in rats. Int J Cancer 91:1–7

Mundhenke C, Thomas JP, Wilding G, Lee FT, Kelzc F, Chappell R, Neides R, Sebree L, Friedl A (2001) Tissue examination to monitor antiangeogenic therapy. Clin Cancer Res 7:3366–3374

Muthukkaruppan VR, Kubai L, Auerbach R (1982) Tumor-induced neovascularization in the mouse eye. J Natl Cancer Inst 69:699–705

Novak K (2002a) Angiogenesis inhibitors revised and revived at AACR. Nature 8:427

O'Reilly MS, Boehm T, Shing Y, Fukai N, Vasios G, Lane WS, Flynn E, Birkhead JR, Olsen BR, Folkman J (1997) Endostatin: an endogenous inhibitor of angiogenesis and tumor growth, Cell 88:277–285

Olsen L, Sherratt JA, Maini PK, Arnold F (1997) A mathematical model for the capillary endothelial cell-extracellular matirix interactions in wound-healing angiogenesis. IMA J Math App Med Biol 14:261–281

Orme ME, Chaplain MAJ (1996). A mathematical model of the first steps of tumor-related angiogenesis: capillary sprout formation and secondary branching. IMA J Math App Med Biol 13:73–98

Orme ME, Chaplain MAJ (1997) Two-dimensional models of tumor angiogenesis and anti-angiogenesis strategies. IMA J Math App Med Biol 14:189–205

Rehn M, Veikkola T, Kukk-Valdre E, Nakamura H, Ilmonen M, Lombardo C, Pihlajaniemi T, Alitalo K, Vuori K (2001) Interaction of endostatin with integrins implicated in angiogenesis. PNAS 98:1024–1029

Sasaki T, Larsson H, Kreuger J, Salmivirta M, Claesson-Welsh L, Lindahl U, Hohenester E, Timpl R (1999) Structural basis and potential role of heparin/heparan sulfate binding to the angiogenesis inhibitor endostatin. EMBO J 18:6240–6248

Sharma A, Jusko, WJ (1998) Characteristics of indirect pharmacodynamic models and applications to clinical drug responses. Br J Clin Pharmacol 45:229–239

Sim BKL, MacDonald NJ, Gubish ER (2000) Angiostatin and endostatin: endogenous inhibitors of tumor growth. Cancer Metastasis Rev 19:181–190

Thomas, JP, Schiller J, Lee F, Perlman S, Friedl A, Winter T, Marnocha R, Arzoomanian R, Alberti D, Binger K, Volkman J, Feierabend C, Tutsch K, Dresen A, Auerbach R, Wilding G (2000) A phase I and pharmacokinetic study of recombinant human endostatin. In: Proc 11th NCI-EORTC-AACR Symp 95:2000. Clin Cancer Res 6[Suppl]